IEEE Robotics and Automation Letters (RA-L) paper, presented at ICRA 2026, Vienna, Austria. Cite as RA-L paper.

A Kinesthetic Teaching Framework for Tasks with Contact Transitions and Time-Optimized Execution

Nikolas Thelenberg[1], *Graduate Student Member, IEEE*, and Christian Ott[2], *Fellow, IEEE*

***Abstract*—In kinesthetic teaching, a robot is manually guided by a human operator to demonstrate a task. Most methods focus on replaying the recorded motion, but are agnostic to contact transitions, which can be critical when interacting with rigid environments. To overcome this limitation, we propose a framework that allows to teach motions in free space as well as in contact while preventing fast unintended contact transitions. This is accomplished by exploiting a projection-based unilateral damping force that increases close to contact. We derive an explicit analytical expression for the damping characteristics to ensure a safe stop before the contact when no further forces act on the robot. Furthermore, after the teaching, the recorded motion data is utilized to generate a time-optimized trajectory based on convex optimization, in which the contact transitions are explicitly considered. We validated our framework in experiments with a torque-controlled manipulator.**

***Index Terms*—Physical human-robot interaction, compliance and impedance control, motion and path planning**

I. Introduction

SINCE the beginning of the century, physical collaboration, interaction, and assistance between humans and robots have received growing interest within the robotics community. Physical human-robot interaction (HRI) has found its way into numerous branches of the field, from industry [1], to medicine [2] and deep-sea applications [3]. One important method in HRI and common practice in these branches is kinesthetic teaching, where the human operator physically guides the robot [4]. Teaching tasks with contact transitions can lead to force peaks that may harm the robot hardware and the environment. This may happen if the operator moves the robot too fast into contact and does not proactively slow down the motion well enough in time.

In this paper we present an impact-aware teaching framework (see Fig. 1), which compared to existing methods bridges from a kinesthetic teaching procedure to time-optimized path execution. As a solution to unintended fast contact transitions, we augment the Cartesian compliance control law with a unilateral damping force. As a damping force, it does not impede the robot's free movement by definition and gets activated only if the end-effector is too close to a rigid environment and its speed is too high. Moreover, the damping force builds up gradually over time. To obtain this behavior, we provide an analytical expression for the required damping factor for different force profiles. This gradual increase results in a smoother and more natural feeling for the user, avoiding abrupt feedback and discontinuities. Therefore, our presented framework

- allows free movement of the robot in its entire workspace,
- prevents fast unintended contact transitions, instead ensures them with reduced velocity, and
- shall feel natural and smooth for the user.

A careful operator will perform the teaching of the contact transitions slowly. However, this can adversely affect task performance, as the teaching speed may differ from the execution speed. The obtained reference trajectory is then executed, whereby the contact transitions are realized at a reduced speed.

II. Related Work

Interaction and collaboration with robots are not meant for experts alone. When novice robot users are supposed to teach tasks on their own, new challenges arise [5]. Especially, the question of safety for both human/ environment and robot arises [6],[7]. Over the years, multiple approaches have been developed to increase safety in HRI. One common technique is to equip the robot with a controller that enables compliant behavior. The impedance controller [8], however, is primarily designed to track a given trajectory by introducing a virtual mass-damper-spring system. Another pre-collision approach is limiting velocity and acceleration [9]. Here, the trajectory is planned by splines satisfying the predefined velocity and acceleration constraints. To fully exploit the potential of both methods, a predefine trajectory is necessary, which consequently reduces their suitability for manual guidance. Dynamical safety zones [10], on the other hand, require a permanent monitoring of the human by a vision sensor. Another approach involves avoiding obstacles by placing potential fields around them [11]. Although this method is physics-inspired and very intuitive, the robot might get stuck in local minima. A modern approach based on control barrier functions (CBF) is presented in [12]. There, a QP-problem is solved online, where the CBF is added as an inequality constraint to keep the end-effector away from the environment. This strategy has already been extended toward barriers around each robot link [13], for safe kinesthetic teaching [14], and learning from demonstrations [15]. Nevertheless, CBF-based controllers have a high computational demand, which can result into issues with real-time performance. When combined with other optimization-based control strategies, conflicts in objective prioritization

Manuscript received: 1 August 2025; Revised 7 November 2025; Accepted 18 December 2025. This paper was recommended for publication by Editor S. Chernova upon evaluation of the Associate Editor and Reviewers' comments. This work was supported in part by he Robot Industry Core Technology Development Program under Grant 00416440 funded by the Korea Ministry of Trade, Industry and Energy (MOTIE).

[1]Nikolas Thelenberg is with the Automation and Control Institute (ACIN), TU Wien, 1040 Vienna, Austria (thelenberg@acin.tuwien.ac.at)

[2]Christian Ott is with the Automation and Control Institute (ACIN), TU Wien, 1040 Vienna, Austria, and with the Institute of Robotics and Mechatronics, German Aerospace Center (DLR), 82234 Weßling, Germany (christian.ott@tuwien.ac.at)

IEEE Robotics and Automation Letters (RA-L) paper, presented at ICRA 2026, Vienna, Austria. Cite as RA-L paper.

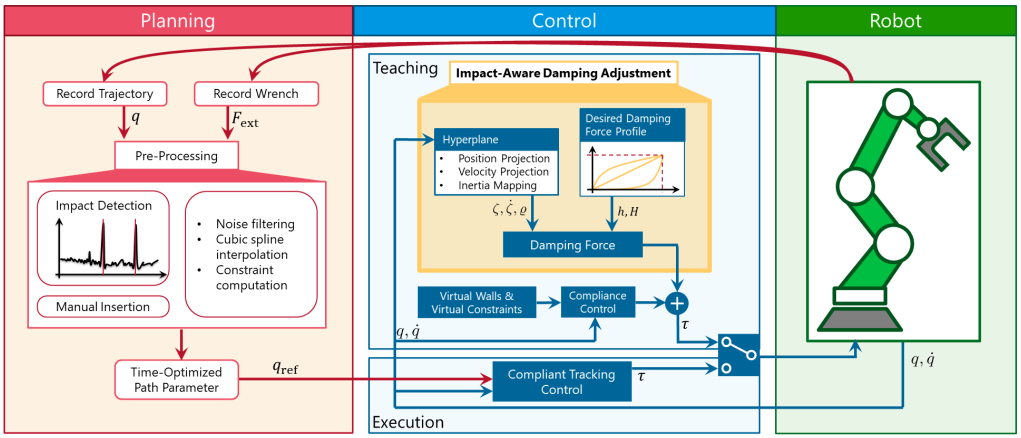

Fig. 1. Conceptual overview of the impact-aware kinesthetic teaching framework

may occur. Further pre- and post-collision control methods are reviewed in [16].

Complementary to the development of frameworks for safe HRI, a distinct line of robotics research has focused on maximizing productivity in industrial applications. As productivity is primarily constrained by speed limitations, minimizing task execution time has been a key topic in robotics research since the early 1970s [17]. One popular approach is to decouple the problem into a path planning phase, which takes geometric aspects into account, and a path tracking phase. In this phase, a time-optimal path parameterization (TOPP) is computed, which considers the manipulator dynamics and constraints [18]. In contrast to the classical numerical integration methods, like [18], a convex optimization based approach to solve the TOPP-problem was introduced in [19].

Our contribution is distinct from the state of the art, since it focuses on contact transitions in both kinesthetic teaching and time-optimal execution.

III. Background

A. Robot Dynamics

The joint space model of a serial robot manipulator with $n \geq 6$ degrees of freedom (DoF) is described by

$$M(q)\ddot{q} + C(q,\dot{q})\dot{q} + g(q) = \tau + J(q)^{\mathrm{T}} F_{\text{ext}}, \tag{1}$$

where $q, \dot{q}, \ddot{q} \in \mathbb{R}^n$ are the vectors of joint positions, velocities and accelerations, respectively. In addition, $M(q) \in \mathbb{R}^{n,n}$ with $M(q) = M(q)^{\mathrm{T}} \succ 0$ denotes the inertia matrix, the expression $C(q,\dot{q})\dot{q} \in \mathbb{R}^n$ contains the Centrifugal and Coriolis terms and $g(q) \in \mathbb{R}^n$ represents the gravity terms. Moreover, $\tau \in \mathbb{R}^n$ expresses the controlled joint torques. The Jacobian $J(q) \in \mathbb{R}^{n,6}$ maps the time-varying generalized external force $F_{\text{ext}} \in \mathbb{R}^6$ at the end-effector to torques in the joint space. For ease of presentation, we assume that the Jacobian $J(q)$ has full row rank for each joint position q.

B. Cartesian Compliance Control

For a simpler representation in task space, the symmetric Cartesian inertia matrix $\Lambda(q) \in \mathbb{R}^{6,6}$ and the Cartesian Coriolis matrix $\Gamma(q,\dot{q}) \in \mathbb{R}^{6,6}$ are defined via

$$\begin{aligned} \Lambda(q) &= \left(JM^{-1}J^{\mathrm{T}}\right)^{-1} \\ \Gamma(q,\dot{q}) &= \Lambda\left(JM^{-1}C - \dot{J}\right)M^{-1}J^{\mathrm{T}}\Lambda. \end{aligned} \tag{2}$$

Applying the forward kinematic map $f(q) = \left[x^{\mathrm{T}}, \varphi^{\mathrm{T}}\right]^{\mathrm{T}}$, the end-effector position $x \in \mathbb{R}^3$ and orientation $\varphi \in \mathbb{R}^3$ are obtained. Depending on the task, we can limit the workspace or lock the orientation of the end-effector by considering virtual walls or virtual constraints. For some given constraint depending reference $x_{\text{ref}}, \varphi_{\text{ref}} \in \mathbb{R}^3$, we introduce the error in the position $\tilde{x}(t) \coloneqq x(t) - x_{\text{ref}}$ and the orientation $\tilde{\varphi}(t) \coloneqq \varphi(t) - \varphi_{\text{ref}}$. Using the task space matrices (2), the compliance control law is stated as

$$\begin{aligned} \tau = {} & g(q) + \tau_{\text{null}} + J^{\mathrm{T}}\Lambda\left(JM^{-1}C - \dot{J}\right)\dot{q} \\ & + J^{\mathrm{T}}\left[-\left(\Gamma + D + \begin{bmatrix} D_{\text{IMP}} & 0 \\ 0 & 0 \end{bmatrix}\right)\begin{pmatrix} \dot{x} \\ \dot{\varphi} \end{pmatrix} - K\begin{pmatrix} \tilde{x} \\ \tilde{\varphi} \end{pmatrix}\right], \end{aligned} \tag{3}$$

where $\tau_{\text{null}} \in \ker(JM^{-1})$ denotes the torque for controlling the null space motion. The stiffness matrix $K = K^{\mathrm{T}} \succcurlyeq 0$ and damping matrix $D = D^{\mathrm{T}} \succcurlyeq 0$ [20] are used optionally to embed the virtual constraints and walls into the control law. Furthermore, the control law (3) contains the term $F_{\text{IMP}} \coloneqq D_{\text{IMP}}\dot{x} \in \mathbb{R}^3$, which acts as a damping force to enable impact-aware teaching. This force is designed to match all the claims presented in the introduction, including unilateralism as well as conditional activation. As will be shown below, the matrix $D_{\text{IMP}} \in \mathbb{R}^{3,3}$ is symmetric, positive semi-definite, and state-dependent, thereby effecting none passivity/stability properties.

IV. Impact-aware Kinesthetic Teaching

In this section, the damping force F_{IMP} and the corresponding matrix D_{IMP} are derived stepwise. For this purpose, the damping behavior in one-dimensional dynamic systems is first studied in more detail.

A. One-dimensional Damping Analysis

1) Mathematical Damping Model: Consider the one-dimensional dynamics of a point mass in free motion with

IEEE Robotics and Automation Letters (RA-L) paper, presented at ICRA 2026, Vienna, Austria. Cite as RA-L paper.

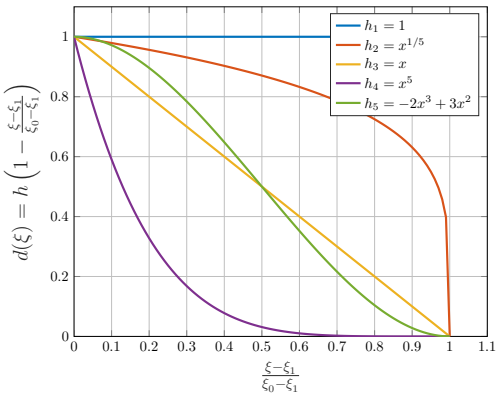

Fig. 2. Course of the damping coefficient $d(\xi)$ with $\delta = 1$ and $\xi \in [\xi_1, \xi_0]$ for various functions h_i,

a dissipation term

$$\eta\ddot{\xi} + d\dot{\xi} = 0, \tag{4}$$

with constant inertia $\eta > 0$ and initial values $\xi(t_0) = \xi_0 > 0$ and $\dot{\xi}(t_0) = \dot{\xi}_0 < 0$, respectively. The damping factor d can be either constant, time-varying or state-dependent. A time-varying approach leads to a non-autonomous system, which is not considered here. Hunt and Crossley [21] proposed a general damping term in their contact model of the form $d\,\xi^{r_1}\dot{\xi}^{r_2}$. Dependent on the parameters r_1 and $r_2 \in \{1, 2\}$, they computed coherent values for the constant d.

Based on their state-dependent contact model, we generalize the damping term in two steps. First, let the force profile $h : \mathbb{R}_0^+ \to \mathbb{R}_0^+$ be a continuous and monotonic increasing function with $h(1) = 1$. Second, concerning the non-zero initial value, the state-depended part is shifted from ξ to $(\xi - \xi_1)/(\xi_0 - \xi_1)$ with $\xi_1 < \xi_0$. Then, we propose a state-dependent damping factor of the form

$$d(\xi) := \delta h\left(1 - \frac{\xi(t) - \xi_1}{\xi_0 - \xi_1}\right) = \delta h\left(\frac{\xi_0 - \xi(t)}{\xi_0 - \xi_1}\right), \tag{5}$$

with constant damping coefficient $\delta > 0$. Due to the variable shift combined with the property $h(1) = 1$, the state ξ_1 denotes the state in which the damping takes effect to the full extent[1]. The impact of the force profile h on the course of the damping factor is visualized in Fig. 2. Note that for $h \equiv 1$, the state-dependent expression vanishes, and only the constant damping coefficient δ remains. In theory, the above-stated conditions on h are sufficient. However, the damping force shall feel smooth and build up gradually over time. We, therefore, restrict ourselves to functions that additionally fulfill $h(0) = 0$. Thus, equation (4) is modified to

$$\eta\ddot{\xi}(t) + \delta h\left(\frac{\xi_0 - \xi(t)}{\xi_0 - \xi_1}\right)\dot{\xi}(t) = 0. \tag{6}$$

2) Unique Damping Value: Since h is continuous, it is integrable and, hence, we define its antiderivative $H(x) = \int_0^x h(\tilde{x})\,\mathrm{d}\tilde{x}$. Note that by definition $H(0) = 0$ holds.

[1]Later, the state ξ_0 is used as a threshold distance to the rigid environment, and ξ_1 as the distance at which the end-effector goes into contact with the rigid environment.

Dividing the differential equation (6) by the inertia $\eta > 0$ and factoring out a time derivative leads to

$$\begin{aligned} 0 &= \ddot{\xi}(t) + \frac{\delta}{\eta} h\left(\frac{\xi_0 - \xi(t)}{\xi_0 - \xi_1}\right)\dot{\xi}(t) \\ &= \frac{\mathrm{d}}{\mathrm{d}t}\left[\dot{\xi}(t) - \frac{\delta(\xi_0 - \xi_1)}{\eta} H\left(\frac{\xi_0 - \xi(t)}{\xi_0 - \xi_1}\right)\right]. \end{aligned}$$

The mean value theorem implies that the interior of the bracket is constant with respect to time, thus,

$$\dot{\xi}(t) - \frac{\delta(\xi_0 - \xi_1)}{\eta} H\left(\frac{\xi_0 - \xi(t)}{\xi_0 - \xi_1}\right) = c = const.$$

holds for $c \in \mathbb{R}$. Since the expression must be valid for all times, it must also be valid for the initial time t_0. We utilize this fact to determine the constant

$$c = \dot{\xi}(t_0) - \frac{\delta(\xi_0 - \xi_1)}{\eta} H\left(\frac{\xi_0 - \xi(t_0)}{\xi_0 - \xi_1}\right) = \dot{\xi}_0 - 0 = \dot{\xi}_0.$$

At this point, the initial value problem with the computed constant $c = \dot{\xi}_0$ and initial condition $\xi(t_0) = \xi_0$

$$\dot{\xi}(t) = \dot{\xi}_0 + \frac{\delta(\xi_0 - \xi_1)}{\eta} H\left(\frac{\xi_0 - \xi(t)}{\xi_0 - \xi_1}\right) \tag{7}$$

remains. Since $h \leq 1$ holds on $[\xi_1, \xi_0]$, the function H is Lipschitz continuous. Therefore, the existence of an unique solution ξ is guaranteed by the Picard–Lindelöf theorem. Note that, up to this point, the damping coefficient $\delta > 0$ can be any positive number. Its value determines the future course of $\xi(t)$ and $\dot{\xi}(t)$, respectively. Let us reverse our perspective and assume that the system has the velocity $\dot{\xi}_1 \in (\dot{\xi}_0, 0)$ at the above introduced state ξ_1. The required time $t_1 > t_0$ and the necessary damping coefficient δ are now both considered unknown. Then, we can solve the non-linear system

$$\xi(t_1, \delta) = \xi_1 \quad \text{and} \quad \dot{\xi}(t_1, \delta) = \dot{\xi}_1 \tag{8}$$

for t_1 and, above all, for the unique damping coefficient δ. Making use of (7)-(8), results in

$$\begin{aligned} \dot{\xi}_1 &\overset{(8)}{=} \dot{\xi}(t_1, \delta) \overset{(7)}{=} \dot{\xi}_0 + \frac{\delta(\xi_0 - \xi_1)}{\eta} H\left(\frac{\xi_0 - \xi(t_1)}{\xi_0 - \xi_1}\right) \\ &\overset{(8)}{=} \dot{\xi}_0 + \frac{\delta(\xi_0 - \xi_1)}{\eta} H(1), \end{aligned}$$

which is solved for the desired damping coefficient

$$\delta = \frac{\eta}{H(1)} \frac{\dot{\xi}_1 - \dot{\xi}_0}{\xi_0 - \xi_1}. \tag{9}$$

For the sake of completeness, the formula for the corresponding time t_1 along with its derivation is found in the Appendix.

Remark 1. *A general closed-form solution of* (6) *as well as an explicit expression for* t_1 *are hard to derive in the general case. However, for the specific functions (a)* $h_1(x) = 1$ *and (b)* $h_3(x) = x$ *both can be obtained analytically. This is achieved by solving* (7) *explicitly for* ξ *and in turn use that function to determine* t_1 *from* (8)*. The results are as follows:*

(a) $h_1(x) = 1$

$$\xi(t) = \xi_0 - \frac{-\eta\dot{\xi}_0}{\delta}\left[1 - \exp\left[\frac{-\delta}{\eta}(t - t_0)\right]\right]$$

IEEE Robotics and Automation Letters (RA-L) paper, presented at ICRA 2026, Vienna, Austria. Cite as RA-L paper.

$$t_1 = t_0 + \frac{\xi_0 - \xi_1}{\dot{\xi}_1 - \dot{\xi}_0} \ln\left(\frac{-\dot{\xi}_0}{-\dot{\xi}_1}\right)$$

(b) $h_3(x) = x$

$$\xi(t) = \xi_0 - \sqrt{\frac{-2\eta\xi_0\dot{\xi}_0}{\delta}} \tanh\left(\sqrt{\frac{-\delta\dot{\xi}_0}{2\eta\xi_0}}(t - t_0)\right)$$

$$t_1 = t_0 + \frac{\xi_0 - \xi_1}{-\dot{\xi}_0}\sqrt{\frac{-\dot{\xi}_0}{\dot{\xi}_1 - \dot{\xi}_0}} \operatorname{artanh}\left(\sqrt{\frac{\dot{\xi}_1 - \dot{\xi}_0}{-\dot{\xi}_0}}\right)$$

Recall that $\dot{\xi}_0 < \dot{\xi}_1 < 0$, so every fraction remains positive.

3) State-dependent Damping Coefficient: The damping should be actively adjusted with the aim of reducing the velocity to a desired velocity $\dot{\xi}_1$ until contact is made. First, the final value is set to zero, i.e. $\xi_1 = 0$, thus, the damping coefficient simplifies to

$$\delta = \frac{\eta}{H(1)} \frac{\dot{\xi}_1 - \dot{\xi}_0}{\xi_0}.$$

Recall that both velocities $\dot{\xi}_0 < \dot{\xi}_1$ have a negative value, hence, the whole expression remains positive. Up next, the initial values are replaced with the current position and velocity, leading to the state-dependent expression

$$\delta = const. \longrightarrow \delta\left(\xi(t), \dot{\xi}(t)\right) = \frac{\eta}{H(1)} \frac{\dot{\xi}_1 - \dot{\xi}(t)}{\xi(t)}.$$

Inserting the state-dependent damping coefficient into (5) yields the closed-loop damping factor

$$d(\xi(t), \dot{\xi}(t)) = \frac{\eta}{H(1)} \frac{\dot{\xi}_1 - \dot{\xi}(t)}{\xi(t)} h\left(\frac{\xi_0 - \xi(t)}{\xi_0}\right). \tag{10}$$

Recall that this state-dependent damping factor is only valid for $\xi(t) \in [0,\ \xi_0]$ and $\dot{\xi}(t) \in [\dot{\xi}_0,\ \dot{\xi}_1]$. This result concludes the analysis of the one-dimensional dynamic system.

B. Projection and Hyperplane

To avoid unintended impacts with a static environment, it is necessary to have a mathematically representation of its location. One approach is modeling it as a three-dimensional hyperplane defined by a unit normal vector $n_{\mathrm{hp}} \in \mathbb{R}^3$ and an offset $p_{\mathrm{hp}} \in \mathbb{R}^3$. The orthogonal (Euclidean) distance $\zeta(t) \in \mathbb{R}$ between the end-effector position x and the hyperplane is obtained via projection as

$$\zeta(t) \coloneqq n_{\mathrm{hp}}^{\mathrm{T}}\left(x(t) - p_{\mathrm{hp}}\right).$$

This allows the velocity $\dot{\zeta}(t) = n_{\mathrm{hp}}^{\mathrm{T}}\dot{x}(t)$ to be derived. A negative velocity $\dot{\zeta} < 0$ indicates movement into the plane, whereas a positive one out of it. For illustrative purposes, a three-dimensional hyperplane, along with the associated projection variables, is sketched in Fig. 3. In addition to kinematic quantities, we use

$$\varrho(q) = \left[\begin{pmatrix} n_{\mathrm{hp}} \\ 0 \end{pmatrix}^{\mathrm{T}} \Lambda(q)^{-1} \begin{pmatrix} n_{\mathrm{hp}} \\ 0 \end{pmatrix}\right]^{-1} \in \mathbb{R} \tag{11}$$

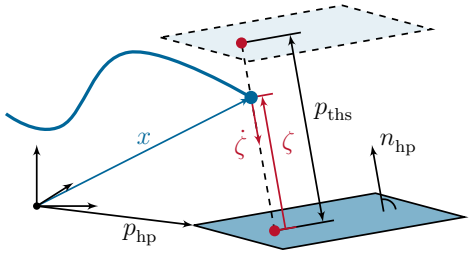

Fig. 3. Three-dimensional hyperplane $(n_{\mathrm{hp}}, p_{\mathrm{hp}})$ and orthogonal projection ζ of the end-effector's position x

to denote the effective inertia projected along the direction of the unit normal vector n_{hp}. Furthermore, any scalar force along the direction of the unit normal vector is transformed into a three-dimensional force in the position space. This fact is utilized to state the damping force, required for kinesthetic teaching as in (3), as

$$F_{\mathrm{IMP}} = n_{\mathrm{hp}} f_{\mathrm{IMP}}, \tag{12}$$

with a scalar force $f_{\mathrm{IMP}} \in \mathbb{R}$. Consequently, the problem of designing a suitable damping force $F_{\mathrm{IMP}} \in \mathbb{R}^3$ simplifies to choose an appropriate scalar force acting along the normal vector of the hyperplane. As a result, all design criteria for F_{IMP}, e.g. unilateralism and smoothness, convey naturally to the scalar f_{IMP}.

C. Damping for Kinesthetic Teaching

The objective is to design a suitable scalar force f_{IMP} that acts along the hyperplane's normal vector. Therefore, it is sufficient to express the force as well as the associated activation and design criteria by the projected scalar quantities.

1) Activation and Thresholds: First, the question is addressed, when the force should be added. To resolve this issue, we define two thresholds. If the conditions

1) $\zeta(t) \leq p_{\mathrm{ths}}$ with $p_{\mathrm{ths}} > 0$ and
2) $\dot{\zeta}(t) < v_{\mathrm{ths}} < 0$

are met, the damping force is added to the control law. The first condition guarantees the free movement in the entire workspace, except close to the hyperplane. In Fig. 3 an projected end-effector is visualized, that satisfies this condition. The second condition generates a unilateral force dependent on the direction of the movement. In other words, if the end-effector moves away from the hyperplane $(\dot{\zeta}(t) > 0)$, the condition is not fulfilled. In addition, the condition ensures that excessive velocities toward the hyperplane are prevented.

2) Damping Force Form: Up to this point, we have formulated conditions, under which the force is applied. Next, the form of the force is stated. Since the force is intended to act as damping, it is defined in the form $f_{\mathrm{IMP}} = d\dot{\zeta}$, depending on the current velocity $\dot{\zeta}$ directed toward the hyperplane. As damping factor d, the result from section IV-A is employed. Therefore, the theoretical result along with the notation is transferred to the current setting.

First, $\zeta(t)$ and $\dot{\zeta}(t)$ are used as position and velocity, respectively. In addition, the constant mass is replaced by the state-dependent effective inertia ϱ from (11). Since the

IEEE Robotics and Automation Letters (RA-L) paper, presented at ICRA 2026, Vienna, Austria. Cite as RA-L paper.

damping force is added, only if $\zeta(t) \leq p_{\text{ths}}$ is fulfilled, the initial position value ξ_0 is replaced by p_{ths}. The remaining parameter $\dot{\zeta}_1$ can be interpreted as the desired velocity or as the remaining velocity at the end of the deceleration. Thus, it is convenient to use the velocity threshold v_{ths}. The sum of all these modifications adds up to

$$f_{\text{IMP}} = \frac{\varrho(q)}{H(1)} \frac{v_{\text{ths}} - \dot{\zeta}(t)}{\zeta(t)} h\left(\frac{p_{\text{ths}} - \zeta(t)}{p_{\text{ths}}}\right) \dot{\zeta}.$$

Inserting that scalar force into (12) and exploiting $\dot{\zeta} = n_{\text{hp}}^{\text{T}} \dot{x}$, results in the damping force

$$\begin{aligned} F_{\text{IMP}} &= \left[\frac{\varrho(q)}{H(1)} \frac{v_{\text{ths}} - \dot{\zeta}(t)}{\zeta(t)} h\left(\frac{p_{\text{ths}} - \zeta(t)}{p_{\text{ths}}}\right)\right] n_{\text{hp}} n_{\text{hp}}^{\text{T}} \dot{x}(t) \\ &= \underbrace{\left(d^*\left(\zeta(t), \dot{\zeta}(t)\right) n_{\text{hp}} n_{\text{hp}}^{\text{T}}\right)}_{=D_{\text{IMP}}} \dot{x}(t). \end{aligned} \tag{13}$$

Note that by design the matrix $D_{\text{IMP}} \in \mathbb{R}^{3,3}$ is symmetric, positive semi-definite and state-dependent.

D. Practical Implementation and Limitations

Close to the hyperplane, the term $(v_{\text{ths}} - \dot{\zeta})/\zeta$ approaches a "zero by zero" limit. Although the underlying differential equation ensures that the damping coefficient remains bounded and well-defined in theory, the position $\zeta(t)$ and velocity $\dot{\zeta}(t)$ are obtained from measurements, which causes numerical issues. In addition, further inaccuracy arises from dividing two small floating-point numbers. Furthermore, the sign change of $\zeta(t)$ after crossing the hyperplane introduces undesired acceleration. For practical implementation, there are two approaches to overcome these issues:

(a) bound the state away from zero with a small positive number ε by $\zeta(t) \leftarrow \max(\varepsilon, \zeta(t))$, or
(b) limit the damping factor between zero and a maximum damping value by $d^* \leftarrow \max(0, \min(d_{\max}, d^*))$.

Both approaches have their advantages and can be applied simultaneously. Using (a) the damping force (13) remains active, even after the hyperplane was crossed. Whereas, (b) constrains the force and, thus, the damping terms in the control law.

The static environment has been modeled with a hyperplane, since this is very intuitive and it has a distinct orthogonal surface vector. It is possible to extended the approach to curved surfaces, as shown in the experiments, as long as a well-defined approach direction is available.

V. Optimization and Execution

Once a task has been successfully taught, the robot can execute it at a higher speed than during the demonstration. The objective is therefore to execute the task as fast as possible. Given are the joint trajectory, torques and end-effector wrenches, which were recorded during the teaching.

A. Gather and Convey Contact Information

Even if we aim for a time-optimized execution, smooth contact transitions during the execution must be ensured. The presence of contacts is crucial and has a major impact on the overall performance. As illustrated in Fig. 1, contact information can be obtained in two ways:

Data Interpretation The proposed method does not prevent contacts in principle. Abrupt or forceful contacts can be identified by detecting large peaks in the rates of change of joint torques or end-effector wrenches, or by using frequency-based techniques [22].

Manual Insertion If the contact has been made smoothly, potential contacts might be undetectable. In such cases, users must add them manually.

Regardless of the chosen method, the joint positions q_j^* corresponding to contact transitions must be included in each of the subsequent processing steps.

B. Pre-process Data and Extract Path Information

Before the time-optimization is executed, some pre-processing offline steps are necessary. The path planning phase, i.e. generating a geometric path, is the main focus in this subsection.

- Since the recorded data contains some noise, we can apply an offline filter to it.
- During teaching, the robot may remain in place, typically at the start or end, resulting in nearly identical joint positions that provide no path information. To address this, points with a geometric distance $\ell_k = \|q_k - q_{k-1}\| < \varepsilon$ are removed.
- If there are still too many data points left, one can reduce them even further, e.g. by only taking every tenth point into account.

From the remaining joint positions, a path $q : [0, 1] \to \mathbb{R}^n$ is generated via cubic spline interpolation [23], which maps the path parameter s to joint positions, i.e. $s \mapsto q(s)$. Since the spline is twice-differentiable, we obtain the first and second derivative $q'(s)$, $q''(s)$ with respect to the path parameter.

C. Incorporate Contact Information

In [19] various constraints on the path parameter s are introduced. Consider the discretization of the path parameter s into grid points $0 = s_0 < \ldots < s_K = 1$. Furthermore, for each joint i the constraint $|\dot{q}_i| \leq \dot{q}_{i,\max}$ is given. This yields the constraint [19]

$$\left(\dot{q}_i(s_k)\right)^2 = \left(q_i'(s_k)\right)^2 \dot{s}_k^2 = \left(q_i'(s_k)\right)^2 b(s_k) \leq \dot{q}_{i,\max}^2. \tag{14}$$

Similarly, we can incorporate a constraint on general task space velocities. A velocity constraint along the hyperplane approach direction is embodied into the algorithm, transforming the stored contact transitions (see Section V-A) into a constraint, with $\dot{\zeta}_{\max}$ denoting the maximum transition velocity and $J_{\text{tra}}(q) \in \mathbb{R}^{3,n}$ representing the translational Jacobian. Since $\dot{\zeta} = n_{\text{hp}}^{\text{T}} \dot{x} = n_{\text{hp}}^{\text{T}} J_{\text{tra}}(q) \dot{q}$ holds, the relation

$$\begin{aligned} \dot{\zeta}^2 &= \left(n_{\text{hp}}^{\text{T}} J_{\text{tra}} \dot{q}(s_k)\right)^2 = \left(n_{\text{hp}}^{\text{T}} J_{\text{tra}}(q(s_k)) q'(s_k)\right)^2 \dot{s}_k^2 \\ &= \left(n_{\text{hp}}^{\text{T}} J_{\text{tra}}(q(s_k)) q'(s_k)\right)^2 b(s_k) \leq \dot{\zeta}_{\max}^2. \end{aligned} \tag{15}$$

yields. At the sampling instance s_k, the end-effector goes into contact at the maximum velocity $\dot{\zeta}_{\max}$. To achieve smoother

IEEE Robotics and Automation Letters (RA-L) paper, presented at ICRA 2026, Vienna, Austria. Cite as RA-L paper.

and more robust transitions, constraint (15) can be applied to neighboring points s_{k-j} and s_{k+j}in addition to s_k. Combining both constraints (14) and (15) to an upper bound $b(s_k) \leq \bar{b}(s_k)$ on the substituted time derivative, we obtain with $i = 1, \ldots, n$

$$\bar{b}(s_k) = \min \left\{ \frac{\dot{\zeta}_{\max}^2}{\left(n_{\mathrm{hp}}^{\mathrm{T}} J_{\mathrm{tra}}(q(s_k))q'(s_k)\right)^2}, \frac{\dot{q}_{i,\max}^2}{\left(q_i'(s_k)\right)^2} \right\}.$$

D. Optimization and Post-Porcessing

We utilize the TOPP-algorithm [19] to generate a time-optimal sequence $b_k = \dot{s}^2(s_k)$. The corresponding time instances starting with $t_0 = 0$ are obtained by

$$t_{k+1} = t_k + 2\frac{s_{k+1} - s_k}{\sqrt{b_{k+1}} + \sqrt{b_k}} \quad \text{for} \quad k = 0, \ldots, K-1.$$

As a result, the time instances t_k are neither equidistant nor do they coincide with the required robot's sampling time. Therefore, we interpolate s_k along the newly computed time grid to obtain the time-optimized path parameter $s(t)$. Combined with the cubic spline $q(s)$ and $q'(s), q''(s)$ from section V-B, we obtain a twice-differentiable joint reference trajectory $t \mapsto q_{\mathrm{ref}}(t) \coloneqq q(s(t))$ as well as

$$t \mapsto \dot{q}_{\mathrm{ref}}(t) = q'(s(t))\dot{s}(t) \qquad \text{and}$$
$$t \mapsto \ddot{q}_{\mathrm{ref}}(t) = q''(s(t))\dot{s}^2(t) + q'(s(t))\ddot{s}(t).$$

A compliant tracking controller can now follow the time-optimized trajectory $q_{\mathrm{ref}}(t)$.

VI. Experiments and Validation

To validate our proposed framework, several experiments have been conducted on a $n = 7$-DoF Franka Research 3 robot. Because of the robot's redundancy, we used null space damping in the compliance control law (3) in all experiments. For the execution phase, we employed a PD+ controller [24] as compliant tracking controller in the joint space. Our proposed damping approach adds only minimal computational overhead, without affecting the control frequency of 1 kHz.

A. Comparison: Free Motion with and without Damping

We compare free motion, constant damping, and four different force profiles of our method. This comparison serves as a baseline validation, since the proposed damping reduces the velocity to a desired value before contact.

1) Setup: To ensure repeatability and reproducibility, a vertical downward motion of the end-effector was performed by a tracking controller without any external force. Then at a height of 0.35m the control law switched to (3). To reduce noise, the velocity $\dot{\zeta}$ was passed through a low-pass filter. The motions were performed for free vertical motion without damping, with constant damping $(d^* = 10, 60)$, and with state-dependent damping (13) for four different force profiles h. The normal vector of the virtual hyperplane pointed in the positive z-direction, $n_{\mathrm{hp}} = [0\ 0\ 1]^{\mathrm{T}}$, and the origin was set to $p_{\mathrm{hp}} = [0\ 0\ 0.1]^{\mathrm{T}}$m. Moreover, the velocity threshold was set to $v_{\mathrm{ths}} = -0.002$m/s and the distance threshold to $p_{\mathrm{ths}} = 0.2$m.

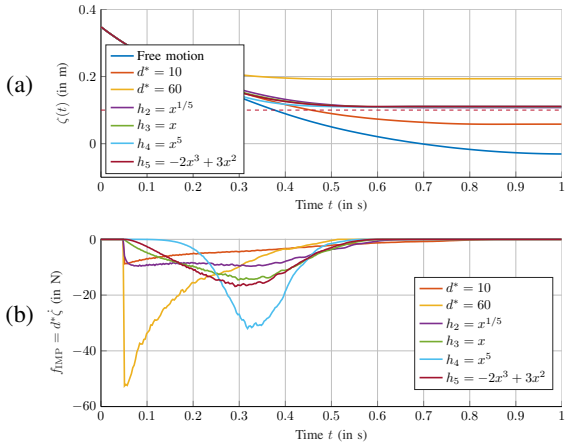

Fig. 4. (a) shows the end-effector position $\zeta(t)$ as well as the virtual hyperplane at 0.1 (dashed red line), and (b) shows the applied scalar damping force f_{IMP} for free motion, constant damping $(d^* = 10, 60)$, and force profiles $h_2, \ldots, h_5$. Free motion and constant damping either overshoot or undershoot the target; constant damping also adds jumps into the control law.

2) Results: The dark blue line in Fig. 4(a) shows the end-effector vertical position in free motion. It moves through the virtual environment at 0.1m (dashed red) by 13cm, where it comes to a halt due to unmodeled friction effects. The two motions with constant damping, however, either overshoot or undershoot the target. All four state-dependent damped motions stop as intended before the hyperplane, regardless of the function h. On the contrary, the force profile h has an significant impact on the course of the scalar damping force f_{IMP}, as seen in Fig. 4(b). Here, the characteristic features of each h_i from Fig. 2 are also recognizable. Furthermore, the suddenly added constant damping terms result in discontinuities in the applied force.

B. User Study

In this user study, we evaluate the practical benefits of the proposed state-dependent damping approach.

1) Setup: All eleven participants were instructed to move the end-effector fast and vertically into contact with a pipe, as shown in Fig. 5, perform a straight wiping motion orthogonal to the surface toward the opposite end, lift the end-effector, and move it back to the starting position. The cycle was repeated four times for each of the investigated methods: (1) gravity compensation, (2) potential field, (3) constant damping $(d = 60)$ and (4) our state-dependent damping with force profile h_5. After each method, participants completed the second part of the NASA Raw TLX, assessing the categories mental demand, physical demand, and performance. In addition, they were asked, "How helpful did you find the robot in performing the contact transitions?" to assess the overall benefit of robot collaboration. All four categories were rated on a scale from 0-20 (low-high), where lower values indicate better performance.

2) Results: The upper part of Table I summarizes the results from the NASA Raw TLX, and the middle row displays the results from the overall benefit of robot collaboration. All median values of our state-dependent damping approach are

IEEE Robotics and Automation Letters (RA-L) paper, presented at ICRA 2026, Vienna, Austria. Cite as RA-L paper.

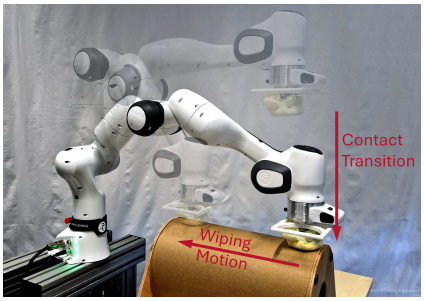

Fig. 5. The used experimental setup for the user study and the validation of the framework

TABLE I
QUALITATIVE AND QUANTITATIVE RESULTS OF THE USER STUDY (ALL VALUES REPRESENT MEDIANS)

	Gravity compensation	Potential field	Constant damping	State-dependent damping (ours)
Mental demand	2	11	2	2
Physical demand	5	7	5	4
Performance	4	8	3	3
Robot collaboration	10	15	7	3
Force magnitude (in N)	34	9.7	30.3	19.6
Extracted energy (in J)	2.7	10.7	2.1	1.9

lower than or equal to those of the other methods, indicating that the proposed method outperforms the others. In addition to the qualitative analysis, we computed quantitative metrics. The first row of the lower part in Table I shows the force magnitudes during contact transition. Moreover, the extracted energy $E_{\text{etra}} = -\int \min\left(0, v^{\mathrm{T}} F_{\text{ext}}\right) \mathrm{d}t$ was computed to quantify the amount of work performed by the user against the robot's motion. As shown in Table I, the state-dependent damping approach achieves the lowest values in both quantitative metrics, except for the potential field method, which is specifically designed to prevent contact and is consistent with the NASA Raw TLX outcomes.

C. Experimental Validation of the Framework

In the last experiment, we tested the framework by teaching a wiping motion on the curved pipe (see Fig. 5).

1) Setup: The motion included three touch-down and lift-off phases. Force profile h_5 was used with velocity threshold $v_{\text{ths}} = -0.002$m/s and distance threshold to $p_{\text{ths}} = 0.15$m. The recorded trajectory consisted of 17,188 data points and is visualized in Fig. 6(a). Based on the derivative of the end-effector forces in Fig. 6(b), the contact transitions were successfully identified and marked with black vertical lines. In the end, 350 sampling points were used to compute the path. For the optimization, $\dot{q}_{\max} = \{2, 1, 1.5, 1.25, 3, 1.5, 3\}$ and $\tau_{\max} = \{87, 87, 87, 87, 12, 12, 12\}$ were taken from the Franka Robotics homepage. The optimization problem was fast solved within 3.03s.

2) Results: In Fig. 6(c), the executed time-optimized reference trajectory q_{ref} is pictured. The original 17s task is completed in approx. 8s. As proposed, the contact transitions are incorporated into the optimization, and thus the robot goes slowly into contact. This velocity reduction is visible by the nearly horizontal lines within the contact boundaries. The entire framework is shown in the attached video.

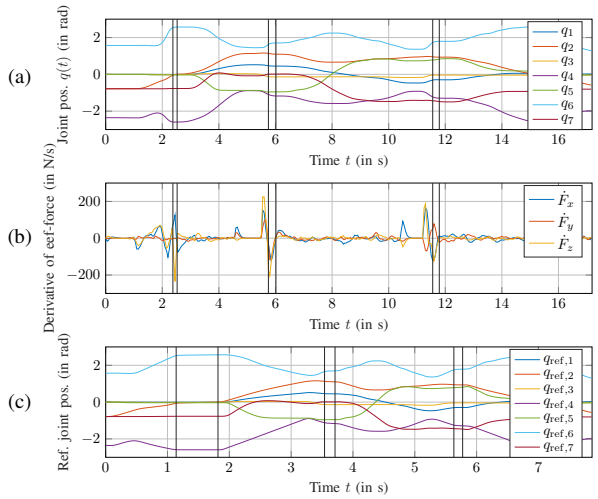

Fig. 6. Wiping motion on a curved pipe: (a) recorded joint positions, (b) derivative of end-effector forces, and (c) time-optimized joint positions. Contacts were identified and their durations were marked with black lines; optimization reduced duration by a factor of 2.14.

VII. Discussion and Limitations

In the previous section, our proposed state-dependent damping approach was successfully validated. The results in qualitative and quantitative metrics indicate the effectiveness of the method. However, the following limitations open up possibilities for future work. The proposed method aims to prevent unintended fast contact transitions by gradual increasing the damping factor for a more natural feeling. However, this excludes task that intentionally aim for violent impacts, e.g. stamping. The proposed method can also not prevent violent user behavior in free motion. For softly demonstrated contact transitions, automatic detection can be challenging and must be augmented manually by the user.

VIII. Conclusion and Outlook

In this paper we presented a kinesthetic teaching framework for tasks with contact transitions and time-optimized execution. The emphasis laid on a damping method based on a state-dependent damping model to prevent fast unintended contact transitions. This feature for kinesthetic teaching as well as our proposed framework were validated in several hands-on experiments. For a visual demonstration, we refer to the attached video.

In our future work, we aim to generalize the approach to multi-point contacts as well as dynamic obstacles. In addition, we aim to extend the framework by teaching impact tasks with faster desired contact transitions. This in return, poses a challenge on the compliant task execution.

Appendix

The damping coefficient δ from (9) is used in the separation of variables of (7) to determine final time t_1 as

$$t_1 - t_0 = \int_{t_0}^{t_1} 1 \, \mathrm{d}\tilde{t} = \int_{\xi_0}^{\xi_1} \frac{1}{\dot{\xi}_0 + \frac{\delta(\xi_0 - \xi_1)}{\eta} H\left(\frac{\xi_0 - \tilde{\xi}}{\xi_0 - \xi_1}\right)} \, \mathrm{d}\tilde{\xi}$$

IEEE Robotics and Automation Letters (RA-L) paper, presented at ICRA 2026, Vienna, Austria. Cite as RA-L paper.

$$\overset{(9)}{=} \int_{\xi_0}^{\xi_1} \frac{1}{\dot{\xi}_0 + (\dot{\xi}_1 - \dot{\xi}_0)\frac{1}{H(1)} H\left(\frac{\xi_0 - \tilde{\xi}}{\xi_0 - \xi_1}\right)} \, \mathrm{d}\tilde{\xi}$$
$$= \frac{\xi_0 - \xi_1}{-\dot{\xi}_0} \int_0^1 \frac{1}{1 - \frac{\dot{\xi}_1 - \dot{\xi}_0}{-\dot{\xi}_0} \frac{H(\bar{\xi})}{H(1)}} \, \mathrm{d}\bar{\xi},$$

where in the last step the substitution of the integration variable $\bar{\xi} := (\xi_0 - \tilde{\xi})/(\xi_0 - \xi_1)$ was used. Before proceeding, we must state a critical assumption regarding the integral.

Assumption 1. *Given is the initial value $\dot{\xi}_0 < 0$, then the final value $\dot{\xi}_1 > \dot{\xi}_0$ fulfills the inequality*

$$\dot{\xi}_0 < \dot{\xi}_1 < 0.$$

Since $\bar{\xi} \leq 1$ holds for all $\bar{\xi} \in [0, 1]$, the continuity of H implies that$H(\bar{\xi}) \leq H(1)$, and, under Assumption 1, the estimation

$$\frac{\dot{\xi}_1 - \dot{\xi}_0}{-\dot{\xi}_0} \frac{H(\bar{\xi})}{H(1)} \leq \frac{\dot{\xi}_1 - \dot{\xi}_0}{-\dot{\xi}_0} < 1$$

holds true. Therefore, the large fraction within the integral is less than one and is replaced with the geometric series $\sum_{k=0}^{\infty} q^k = 1/(1-q)$ for $|q| < 1$, which leads to

$$t_1 = t_0 + \frac{\xi_0 - \xi_1}{-\dot{\xi}_0} \int_0^1 \sum_{k=0}^{\infty} \left[\frac{\dot{\xi}_1 - \dot{\xi}_0}{-\dot{\xi}_0} \frac{H(\bar{\xi})}{H(1)}\right]^k \mathrm{d}\bar{\xi}$$
$$= t_0 + \frac{\xi_0 - \xi_1}{-\dot{\xi}_0} \sum_{k=0}^{\infty} \left[\frac{\dot{\xi}_1 - \dot{\xi}_0}{-\dot{\xi}_0}\right]^k \int_0^1 \left[\frac{H\left(\bar{\xi}\right)}{H(1)}\right]^k \mathrm{d}\bar{\xi}.$$

By the Weierstrass M-test the geometric series converges uniformly, which we utilize to reverse the order of integral and series. Since t_1 is largely determined by H, obtaining a closed-form solution that avoids both integrals and series is challenging. However, Assumption 1 is a sufficient condition for the existence of t_1. As $H(\bar{\xi}) \leq H(1)$ is valid for all $\bar{\xi} \in [0, 1]$, the integral is estimated upwards by

$$t_1 \leq t_0 + \frac{\xi_0 - \xi_1}{-\dot{\xi}_0} \sum_{k=0}^{\infty} \left[\frac{\dot{\xi}_1 - \dot{\xi}_0}{-\dot{\xi}_0}\right]^k \int_0^1 1^k \, \mathrm{d}\bar{\xi}$$
$$= t_0 + \frac{\xi_0 - \xi_1}{-\dot{\xi}_0} \sum_{k=0}^{\infty} \left[\frac{\dot{\xi}_1 - \dot{\xi}_0}{-\dot{\xi}_0}\right]^k = t_0 + \frac{\xi_0 - \xi_1}{-\dot{\xi}_1} < \infty.$$

ACKNOWLEDGMENT

The authors acknowledge TU Wien Bibliothek for financial support through its Open Access Funding Programme.

REFERENCES

[1] C. Schou, J. S. Damgaard, S. Bøgh, and O. Madsen, "Human-robot interface for instructing industrial tasks using kinesthetic teaching," in *IEEE ISR 2013*. IEEE, 2013, pp. 1–6.

[2] L. Xiong, C. B. Chng, C. K. Chui, P. Yu, and Y. Li, "Shared control of a medical robot with haptic guidance," *International Journal of Computer Assisted Radiology and Surgery*, vol. 12, no. 1, pp. 137–147, Jan. 2017, publisher: Springer Science and Business Media LLC.

[3] G. Brantner and O. Khatib, "Controlling Ocean One: Human–robot collaboration for deep-sea manipulation," *Journal of Field Robotics*, vol. 38, no. 1, pp. 28–51, 2021.

[4] D. Lee and C. Ott, "Incremental kinesthetic teaching of motion primitives using the motion refinement tube," *Autonomous Robots*, vol. 31, no. 2-3, pp. 115–131, Oct. 2011.

[5] P. Aliasghari, M. Ghafurian, C. L. Nehaniv, and K. Dautenhahn, "How Non-experts Kinesthetically Teach a Robot over Multiple Sessions: Diversity in Teaching Styles and Effects on Performance," *International Journal of Social Robotics*, vol. 16, no. 11-12, pp. 2079–2105, 2024.

[6] A. Bicchi, M. A. Peshkin, and J. E. Colgate, "Safety for Physical Human–Robot Interaction," in *Springer Handbook of Robotics*. Springer, Berlin, Heidelberg, 2008, pp. 1335–1348.

[7] A. Zacharaki, I. Kostavelis, A. Gasteratos, and I. Dokas, "Safety bounds in human robot interaction: A survey," *Safety Science*, vol. 127, p. 104667, Jul. 2020.

[8] N. Hogan, "Impedance Control: An Approach to Manipulation," in *1984 American Control Conference*, Jun. 1984, pp. 304–313.

[9] X. Broquere, D. Sidobre, and I. Herrera-Aguilar, "Soft motion trajectory planner for service manipulator robot," in *IEEE/RSJ International Conference on Intelligent Robots and Systems*, 2008, pp. 2808–2813.

[10] C. Vogel, C. Walter, and N. Elkmann, "A projection-based sensor system for safe physical human-robot collaboration," in *IEEE/RSJ Int. Conf. on Intelligent Robots and Systems*, 2013, pp. 5359–5364.

[11] O. Khatib, "Real-time obstacle avoidance for manipulators and mobile robots," *The international journal of robotics research*, vol. 5, no. 1, pp. 90–98, 1986.

[12] M. Rauscher, M. Kimmel, and S. Hirche, "Constrained robot control using control barrier functions," in *IEEE/RSJ International Conference on Intelligent Robots and Systems (IROS)*, 2016.

[13] C. T. Landi, F. Ferraguti, S. Costi, M. Bonfe, and C. Secchi, "Safety Barrier Functions for Human-Robot Interaction with Industrial Manipulators," in *2019 18th European Control Conference*, pp. 2565–2570.

[14] J. M. S. Ducaju, B. Olofsson, A. Robertsson, and R. Johansson, "Robot Cartesian Compliance Variation for Safe Kinesthetic Teaching using Safety Control Barrier Functions," in *IEEE 18th Int. Conf. on Automation Science and Engineering*, 2022, pp. 2259–2266.

[15] Y. Yang, L. Chen, Z. Zaidi, S. Van Waveren, A. Krishna, and M. Gombolay, "Enhancing Safety in Learning from Demonstration Algorithms via Control Barrier Function Shielding," in *2024 ACM/IEEE International Conference on Human-Robot Interaction*. Boulder CO USA: ACM, Mar. 2024, pp. 820–829.

[16] P. A. Lasota, T. Fong, and J. A. Shah, "A survey of methods for safe human-robot interaction," *Foundations and Trends in Robotics*, vol. 5, no. 4, pp. 261–349, 2017.

[17] M. E. Kahn and B. Roth, "The Near-Minimum-Time Control Of Open-Loop Articulated Kinematic Chains," *Journal of Dynamic Systems, Measurement, and Control*, vol. 93, no. 3, pp. 164–172, 1971.

[18] J. Bobrow, S. Dubowsky, and J. Gibson, "Time-Optimal Control of Robotic Manipulators Along Specified Paths," *The International Journal of Robotics Research*, vol. 4, no. 3, pp. 3–17, Sep. 1985.

[19] D. Verscheure, B. Demeulenaere, J. Swevers, J. De Schutter, and M. Diehl, "Time-Optimal Path Tracking for Robots: A Convex Optimization Approach," *IEEE Transactions on Automatic Control*, vol. 54, no. 10, pp. 2318–2327, Oct. 2009.

[20] B. Siciliano, L. Sciavicco, L. Villani, and G. Oriolo, *Robotics: modelling, planning and contro*, ser. Advanced Textbooks in Control and Signal Processing. London: Springer, 2009.

[21] K. H. Hunt and F. R. E. Crossley, "Coefficient of Restitution Interpreted as Damping in Vibroimpact," *Journal of Applied Mechanics*, vol. 42, no. 2, pp. 440–445, Jun. 1975.

[22] J. M. Salt Ducaju, B. Olofsson, A. Robertsson, and R. Johansson, "Fast Contact Detection and Classification for Kinesthetic Teaching in Robots using only Embedded Sensors," in *31st IEEE Int. Conf. on Robot and Human Interactive Communication*, 2022, pp. 1138–1145.

[23] G. Micula and S. Micula, *Handbook of Splines*. Springer Dordrecht, 1999.

[24] B. Paden and R. Panja, "Globally asymptotically stable 'PD+' controller for robot manipulators," *International Journal of Control*, vol. 47, no. 6, pp. 1697–1712, Jun. 1988.